P1.20

THE NOAA-9 EARTH RADIATION BUDGET EXPERIMENT WIDE FIELD-OF-VIEW DATA SET

Kathryn A. Bush*,
Science Applications International Corporation
G. Louis Smith,
Virginia Polytechnic Institute and State University
David F. Young
Atmospheric Sciences Division,
Langley Research Center, NASA, Hampton, Virginia

1. INTRODUCTION

The Earth Radiation Budget Experiment (ERBE) consisted of wide field-of-view (WFOV) radiometers (Luther, 1986) and scanning radiometers for measuring outgoing longwave radiation and solar radiation reflected from the Earth (Barkstrom and Smith, 1986). These instruments were carried by the dedicated Earth Radiation Budget Satellite (ERBS) and by the NOAA-9 and -10 operational spacecraft. The WFOV radiometers provided data from which instantaneous fluxes at the top of the atmosphere (TOA) are computed by use of a numerical filter algorithm (Smith et al., 1986). Monthly mean fluxes over a 5-degree equal angle grid are computed from the instantaneous TOA fluxes (Brooks et al., 1986). The WFOV radiometers aboard the NOAA-9 spacecraft operated from February 1985 through December 1992, at which time a failure of the shortwave radiometer ended the usable data after nearly 8 years. This paper examines the monthly mean products from that data set.

Bush et al. (1999) describe the data set from the ERBS WFOV radiometers, which have operated since November 1984. Those data cover the Earth from the Equator to a latitude of 60^{o} in both hemispheres. The NOAA-9 WFOV measurements cover the globe up to 85^{o}. As a system, the two NOAA spacecraft and the ERBS provide excellent temporal and spatial coverage (Harrison et al., 1983). However, the NOAA-9 orbit slowly precessed over this period so that the local time of Equator crossing of the ascending node varied from 1400 hours at the beginning to 2000 hours at the end of the period. This precession of the NOAA-9 orbit introduced artifacts into the monthly data products, but physical interannual variations of radiative fluxes can still be retrieved from the data.

2. SPACECRAFT ORBIT

Figure 1 shows the local solar time of the ascending node of the NOAA-9 orbit. There is a long term trend as the orbit precesses approximately 1 hour of Equator crossing time per year over the data period. There are also small annual and semiannual cycles, mainly due to the solar declination annual variation.

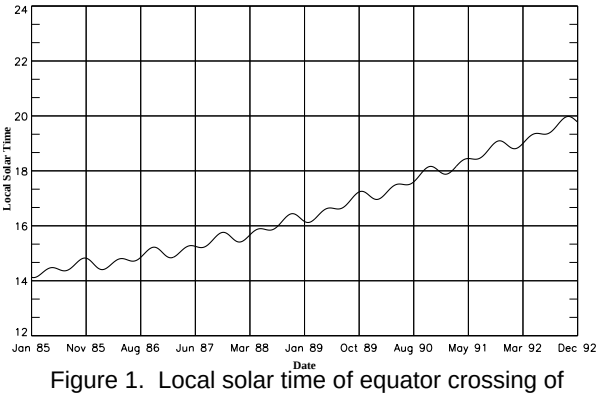

Figure 1. Local solar time of equator crossing of ascending node for NOAA-9 spacecraft.

The latitude range for which the reflected shortwave radiation is measured varies with the solar declination and the Equator crossing local time. Figure 2 shows the latitude range of measurements over the data period. From September 1990 through July 1991 the spacecraft was in a near-terminator orbit. Also, no data are available for May - July 1991. As the orbit approached the terminator, the coverage of the Southern Hemisphere diminished until the terminator crossed the Equator, at which time the coverage of the Northern Hemisphere decreased.

3. ANALYSIS METHOD

In order to examine the interannual variability of the data, monthly means of outgoing longwave radiation (OLR) and reflected shortwave radiation (SWR) for 5^{o} regions, computed using the numerical filter algorithm, were obtained from the ERBE S-10 data products. This set contained data for 89 months. Climatological mean maps for each month of the year were computed, then the anomaly map for each month was computed. These anomaly maps are the basis for interannual variability studies.

Principal components (PCs) and empirical orthogonal functions (EOFs) were calculated for the OLR and for

*Corresponding author address: Kathryn A. Bush, SAIC, 1 Enterprise Parkway, Suite 300, Hampton, VA 23888
email: k.a.bush@larc.nasa.gov

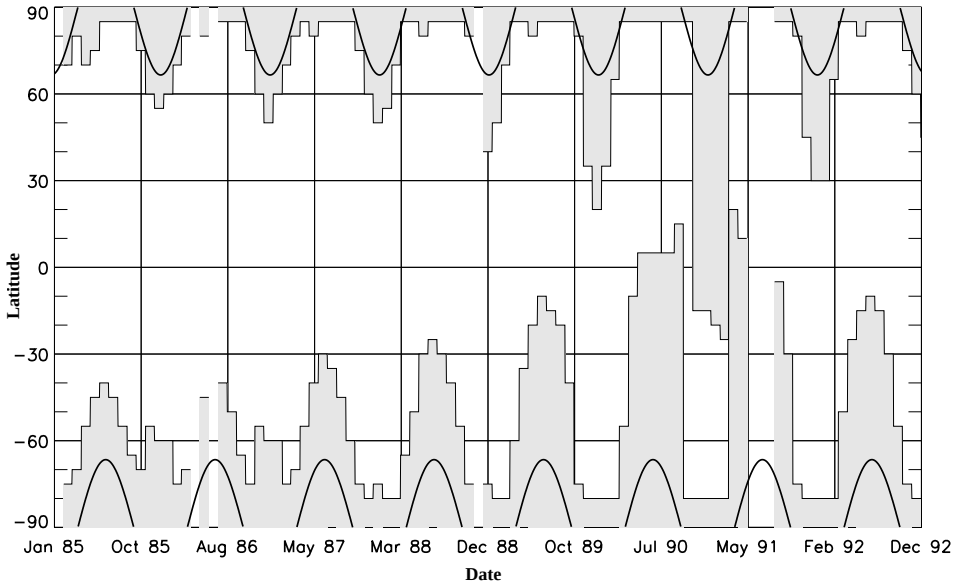

Figure 2. Latitude coverage of NOAA-9 shortwave measurements. Shaded regions indicate no measurements. Solid curves at top and bottom of the figure indicate solar declination.

the SWR. A covariance matrix in the time domain was calculated by the sum of the area-weighted squares of the anomalies. Because of the gaps of coverage at latitudes greater than 60^o in each hemisphere, only regions with latitudes less than 60^o were included in this analysis. For the SWR case, several elements of this matrix were undefined for the 89 month data set due to the lack of coverage during months close to the terminator. Eight months were deleted from the analysis and the covariance matrix was calculated for this 81-month data set. The eigenvectors of the covariance matrix are the principal components and their projections onto the anomaly matrix are the EOF maps.

4. RESULTS

Figure 3 shows the time variation of the first 3 PCs for the OLR case. Each PC is scaled such that it is the RMS value over the spatial domain from 60^o North to 60^o South. PC-1 corresponds to the Southern Oscillation (Tahiti-Darwin pressure difference) time hstory. It has a range of 12 W-m^{-2} and accounts for 12% of the variance of the monthly anomalies of OLR. Figure 4 shows EOF-1 map for OLR. The EOF map is scaled in terms of standard deviations. The ENSO pattern is clear.

PC-2 is an artifact of precession and accounts for 9% of the OLR variance. EOF-2 for OLR (not shown) is primarily a zonal pattern which is small north of 45^o and increases toward the south.

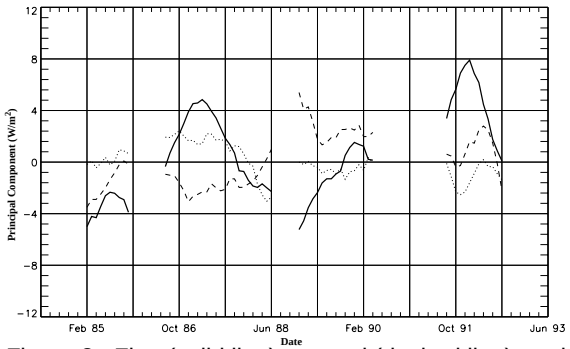

Figure 3. First (solid line), second (dashed line), and third (dotted line) principal components of NOAA-9 deseasonalized OLR, filtered with a 5-month running mean.

PC-3 has a range less than 5 W-m^{-2} and accounts for less than 5% of the OLR variance. The EOF-3 map, shown in figure 5, may be related to the Pacific-Indian Ocean coupling found by Bush et al. (1999) in the ERBS data set.

For the SWR case, figure 6 shows the time variation of the first 3 PCs. The first is an artifact due to the precession and has a total range of 16 W-m^{-2}. EOF-1 for SWR is primarily a bias over the spatial domain. PC-2 has minima at the times of the 1986-87 and 1991-92 ENSOs. Figure 7 is the map of EOF-2 for shortwave.

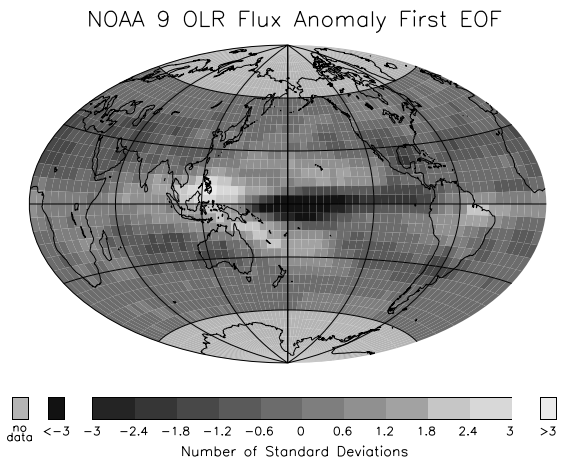

Figure 4. Map of first EOF for NOAA-9 deseasonalized OLR.

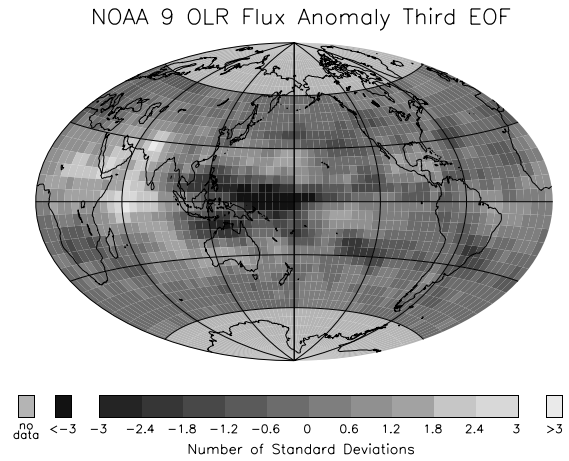

Figure 5. Map of third EOF for NOAA-9 deseasonalized OLR.

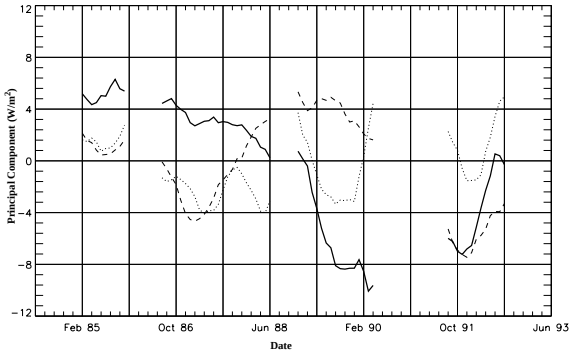

Figure 6. First (solid line), second (dashed line), and third (dotted line) principal components of NOAA-9 deseasonalized SWR, filtered with a 5-month running mean.

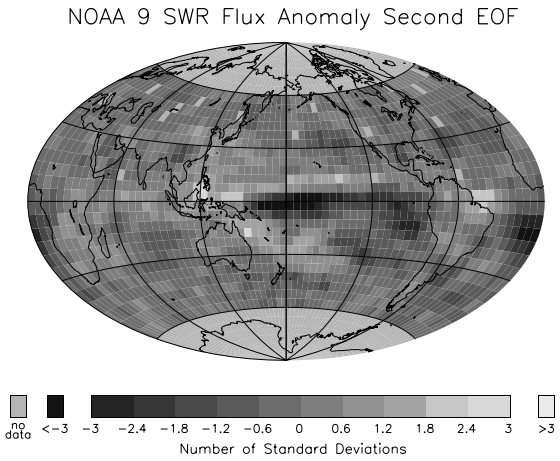

Figure 7. Map of second EOF for NOAA-9 deseasonalized SWR.

PC-3 for the SWR ranges between +/-4 W-m^{-2} and shows annual cycles. EOF-3 is low in the Northern Hemisphere and high in the Southern Hemisphere. PC-3 and EOF-3 appear to be artifacts due to the variation of angle between the orbit plane and the Sun, which varies with solar declination.

5. DISCUSSION

Due to the orbital precession, the data product for the monthly mean SWR contains effects due to the diurnal cycle of radiation as sampled by this orbit, together with errors of the model of the albedo variation with solar zenith angle, which is used to compute the daily mean from the instantaneous value of SWR. The consequences of these errors would not be so large for the planned orbit. However, the errors which are incurred in the interpolation from measurement time though the remainder of the day grow considerably as measurement time nears sunrise or sunset. Neither the algorithms nor the models have been changed in view of the precession. It is recommended that ERBE data be used to upgrade the models and the algorithms in order to reduce the effects of precession on the monthly mean data products. One aspect of the algorithm to be addressed is the limit of local time of measurement beyond which daily means of SWR will be computed.

6. ACKNOWLEDGEMENTS

This work was supported by the Earth Science Enterprise of NASA through Langley Research Center by contract NAS1-19579 to Science Applications International Corporation and grant NAG1-1959 to Virginia Polytechnic Institute and State University. We also thank Jonathan White and Dena Banks of SAIC for preparation of the figures and manuscript.

7. REFERENCES

Barkstrom, B. R. and G. L. Smith, 1986: The Earth Radiation Budget Experiment: Science and Implementation, *Rev. of Geophys., 24*, 379-390.

Brooks, D. R., E. F. Harrison, P. Minnis, J. T. Suttles and R. S. Kandel, 1986: Development of algorithms for understanding the temporal and spatial variability of Earth radiation balance, *Rev. Geophys., 24*, 422-438.

Bush, K. A., G. L. Smith, D. A. Rutan, B. R. Barkstrom, R. B. Lee, III and D. F. Young, 1999: The Earth Radiation Budget Satellite 13-year data set, *Proc. 10th Symposium on Global Change Studies, 10-15 Jan. 1999, Dallas, TX by* Amer. Met. Soc., Boston.

Harrison, E. F., P. Minnis, and G. G. Gibson, 1983: Orbital and cloud cover sampling analyses for multisatellite Earth radiation budget experiments, *J. Spacecraft and Rockets, 20*, 491-495.

Luther, M. R., J. E. Cooper and G. R. Taylor, 1986: The Earth Radiation Budget Experiment nonscanning instrument, *Rev. of Geophys., 24*, 391-399.

Smith, G. L., R. N. Green, E. Raschke, L. M. Avis, J. T. Suttles, B. A. Wielicki and R. Davies, 1986: Inversion methods for satellite studies of the Earth's radiation budget: Development of algorithms for the ERBE mission, *Rev. Geophys, 24*, 407-421.